

# Evidence of Spin-Interference Effects in Exclusive $J/\psi \rightarrow e^+e^-$ Photoproduction in Ultraperipheral Heavy-Ion Collisions

(The STAR Collaboration)

We report the first evidence of spin interference in exclusive  $J/\psi \rightarrow e^+e^-$  photoproduction in ultraperipheral Au+Au and isobar (Ru+Ru, Zr+Zr) collisions ( $\sqrt{s_{NN}} = 200$  GeV) at STAR. A negative  $\cos(2\phi)$  modulation is observed for  $p_T < 100$  MeV/c, opposite in sign to that in  $\rho^0 \rightarrow \pi^+\pi^-$  photoproduction. This establishes for the first time that the interference sign is controlled by the spin structure of the final-state daughters, resolving the ambiguity present in the all-boson  $\rho^0$  channel. The compact  $J/\psi$  probes gluon distributions at perturbative scales, resulting in a weaker modulation and providing stringent constraints on Color Glass Condensate calculations. These findings demonstrate that spin-dependent interference in heavy vector mesons provides a new, experimentally accessible handle on gluon structure beyond traditional cross-section measurements.

Photon-induced processes can reveal the fundamental structures in nature. From crystallography to the cosmic microwave background, the ability of photons to probe hidden structures has shaped our understanding of the universe. In nuclear and particle physics, this idea takes on a new form: by accelerating electrons or ions, a high-energy collider creates intense electromagnetic fields that act like beams of photons. In electron–proton and electron–ion collisions, most famously studied at HERA and envisioned at the future Electron–Ion Collider (EIC), the photon is emitted by the electron and probes the internal structure of the target [1]. Without an  $e+A$  collider, similar measurements can be performed in ultraperipheral heavy ion collisions (UPCs) where the ions don’t interact hadronically, albeit with less control over initial kinematics. Ultrarelativistic ions generate strong electromagnetic fields due to their large charge and Lorentz boost, producing a flux of quasireal photons via the Weizsäcker–Williams (WW) approximation [2, 3]. When two ions pass without colliding, a photon from the projectile may fluctuate into a quark–antiquark pair and interact with the gluon field of the target, producing short-lived particles that carry the quantum numbers of the photon and encode the spatial and momentum structure of the gluon field in the target nucleus.

The process is known as exclusive photoproduction, *e.g.*,  $\gamma^* + A \rightarrow V + A$ , where  $V$  is a vector meson such as  $\rho^0$ ,  $\phi$ , or  $J/\psi$ , and  $\gamma^*$  is a quasireal photon [2]. In this reaction, the photon may scatter off the gluon field of the target nucleus, either coherently, involving the entire nucleus, or incoherently, on localized substructures. The momentum transfer ( $t$ ) distribution of the produced vector meson ( $d\sigma/dt$ ) is conjugate to the target’s spatial gluon density, encoding both the overall nuclear geometry in coherent events and small-scale fluctuations in incoherent processes [4–8]. These processes have been studied extensively in RHIC and the LHC experiments [9–21]. Nevertheless, there are several open questions [22–25] regarding the gluon density distribution.

Notably, photons in UPCs are linearly polarized in the transverse plane, as demonstrated by previous STAR

experiment [26]. In vector meson photoproduction, the spin-1 photon transfers its polarization to the produced meson, aligning their spin directions. When the vector meson decays, its daughters’ momenta tend to align with the parent spin due to conservation of angular momentum, resulting in an anisotropic azimuthal distribution:

$$\frac{dN}{d\phi} \propto 1 + a_2 \cos(2\phi) \quad (1)$$

Here,  $\phi$  is the angle of vector meson momentum ( $\vec{p}$ ) relative to the parent spin direction or photon polarization axis, and  $a_2$  is the modulation amplitude. In UPCs, photon polarization is approximately aligned with the impact parameter ( $\vec{b}$ ), which is random from event to event and not directly accessible experimentally. Averaging over many events with random polarization orientations would wash out any  $\cos(2\phi)$  asymmetry.

In coherent vector-meson production, where both nuclei remain intact, it is unknown which one emits the photon and which acts as the target. This two-path ambiguity contributes at the amplitude level; and a phase difference,  $e^{i\vec{p}\cdot\vec{b}}$ , between the wave functions in these two paths [27–29] leads to quantum interference [30, 31]. Hence the  $\cos(2\phi)$  asymmetry survives [29], analogous to a double-slit interference pattern in optics [27]. In experimental measurements of  $\phi$ , the daughters’ momenta are used as a proxy for the spin of the vector meson or the direction of the photon polarization. Experimentally,  $\phi$  is therefore taken to be the angle in the transverse plane between the vector meson’s momentum and the relative momentum of its decay daughters [29, 32]:

$$\cos \phi = \frac{(\vec{p}_{T1} + \vec{p}_{T2}) \cdot (\vec{p}_{T1} - \vec{p}_{T2})}{|\vec{p}_{T1} + \vec{p}_{T2}| |\vec{p}_{T1} - \vec{p}_{T2}|} \quad (2)$$

where  $\vec{p}_{T1}$  and  $\vec{p}_{T2}$  are transverse momenta of the daughters. Refs. [29, 30, 33] argue that short-lived vector mesons decay before amplitudes from the two sources can overlap, preventing direct interference. However, the decay products are emitted in an entangled state, and the interference arises from collapsing the full final-state

wavefunction. The recently developed Entanglement-Enabled Intensity Interferometry (E<sup>2</sup>I<sup>2</sup>) framework [34] formalizes this idea, proposing that vector meson decay acts as an “entanglement filter,” leading to interference between the daughter particle wave functions. As a result, the phase information imprinted during meson production is preserved and transmitted into the decay distribution, which makes the interference sustainable. This perspective extends the conventional interpretation by viewing the  $\rho^0$  or  $J/\psi$  not as isolated particles with definite polarization, but as entangled two-particle states formed by their decay products at the amplitude level. Conceptually, the joint quantum state of the decay daughters retains the memory of the production phase difference. The entanglement between the two decay products arises not from a novel mechanism, but rather is an inevitable consequence of the conservation of total angular momentum and parity during the decay.

A  $\cos(2\phi)$  modulation, attributed to spin interference, was observed in exclusive  $\rho^0$  production in ultra-peripheral Au+Au [29] and also in Pb+Pb collisions [32]. The interference arises from the overlap of two spatially separated  $\rho^0$  wave functions produced coherently in the two nuclei, which are tens of femtometers apart (Fig. 1 (a)), far exceeding the  $\approx 1$  fm lifetime travel distance of the  $\rho^0$  [29]. Consequently, the observed modulation must be transmitted through the entangled  $\pi^+\pi^-$  daughters, as described by the E<sup>2</sup>I<sup>2</sup> framework [34]. This observation has enabled nuclear “tomography,” as the interference pattern is sensitive to the nuclear geometry and size [29].

However, the  $\rho^0$  measurements leave key questions unresolved, due to fundamental limitations of the meson and its decay channel. Because the  $\rho^0$  and its  $\pi^+\pi^-$  daughters are bosons, the parent- and final-state contributions are experimentally indistinguishable, leaving no testable signature to confirm the specific - or indeed any - role of the daughters. Beyond such interpretational challenges, the  $\rho^0$  also faces limitations as a probe of gluon distributions. Its low mass and large transverse dipole size make it less sensitive to small- $x$  evolution, and obscures its suitability for studying saturation effects [34]. In contrast,  $J/\psi \rightarrow e^+e^-$  photoproduction provides a cleaner probe that resolves these issues. Its long lifetime ( $c\tau \approx 2160$  fm) allows the quantum state to evolve and interfere well beyond the nuclear volume (Fig. 1 (b)). In this case, the fermionic nature of the  $e^+e^-$  daughters imposes a definite sign on the  $\cos(2\phi)$  modulation, providing a clear, testable fingerprint of the daughters’ role and removing the ambiguity present in the  $\rho^0$  channel. Additionally, its mass justifies perturbative treatment without suppressing sensitivity to the saturation regime [35].

In this Letter, we present the first measurement of the spin-interference angular modulation for exclusive  $J/\psi$  photoproduction in UPCs, comparing Au+Au to isobaric (Ru+Ru and Zr+Zr) collisions at  $\sqrt{s_{NN}} = 200$  GeV. The

results are contrasted with the existing  $\rho^0$  measurements and compared with CGC-based model expectations.

We analyze UPC events from Au+Au, Ru+Ru and Zr+Zr collisions at  $\sqrt{s_{NN}} = 200$  GeV collected with the STAR detector [36], with an integrated luminosity of 13.5, 4 and 3.9 nb<sup>-1</sup>, respectively. Charged particle tracking, including transverse momentum reconstruction, is carried out using the time projection chamber (TPC) [37], which operates within a 0.5 T solenoidal magnetic field. The TPC extends radially from 50 to 200 cm from the beam axis, covering pseudorapidities  $|\eta| < 1.0$  over the azimuthal range  $0 < \phi < 2\pi$ . It also provides ionization energy loss ( $dE/dx$ ) measurements for particle identification. A barrel electromagnetic calorimeter (BEMC) [38] surrounding the TPC is a lead-scintillator sampling calorimeter segmented into 4800 optically isolated towers within  $|\eta| < 1.0$ . Positioned radially between the TPC and BEMC, the time-of-flight (TOF) system [39] is finely segmented in both  $\eta$  and  $\phi$ , offering fast trigger signals for charged particles in the range  $|\eta| < 0.9$ . Additionally, two beam-beam counters (BBCs) [40] are located on either side of the STAR detector, covering the range  $3.4 < |\eta| < 5.0$ , while two zero-degree calorimeters (ZDCs) [41], placed at  $|\eta| > 6.7$ , are used to monitor luminosity while detecting forward neutrons. To trigger the UPC events, we require forward neutron showers in both ZDCs, limited activity in TOF and BEMC, and no signal in the BBCs. The analysis aims to select events with exclusive  $J/\psi \rightarrow e^+e^-$  production, which requires that there be only two tracks in a single event. For very low- $p_T$   $J/\psi$  candidates, the decay tracks exhibit an approximately back-to-back topology, typically leaving hits in opposite sextants of the BEMC [11, 12].

We select UPC events which include a pair of tracks with a reconstructed vertex positioned longitudinally within  $\pm 100$  cm of the center of the TPC. To ensure adequate momentum resolution, each track must have at least 15 recorded hits out of a possible 45, along with a minimum of 11 hits for an ionization energy loss ( $dE/dx$ ) measurement to maintain reliable  $dE/dx$  resolution. Tracks are also required to point to a BEMC cluster for trigger consistency. The selection of electron pairs relies on track-based  $dE/dx$  values, with pion contamination being the primary background at  $p_T \sim 1.5$  GeV/ $c$ . The variable  $n\sigma_e$  ( $n\sigma_\pi$ ) quantifies the deviation of the measured  $dE/dx$  from the expected electron ( $\pi$ ) hypothesis, expressed in terms of standard deviations from the theoretical mean. A pair selection variable is defined as:  $\chi_{ee}^2 = n_{\sigma,e1}^2 + n_{\sigma,e2}^2$  for tracks 1 and 2, with a similar formulation applied under the pion pair hypothesis. Electron pair candidates are identified by requiring  $\chi_{ee}^2 < 10$ , while pion pair contamination is suppressed by enforcing the condition  $\chi_{ee}^2 < \chi_{\pi\pi}^2$ . These selection criteria are applied independently to opposite-sign (+-) and like-sign (++, --) pairs. The like-sign distributions are

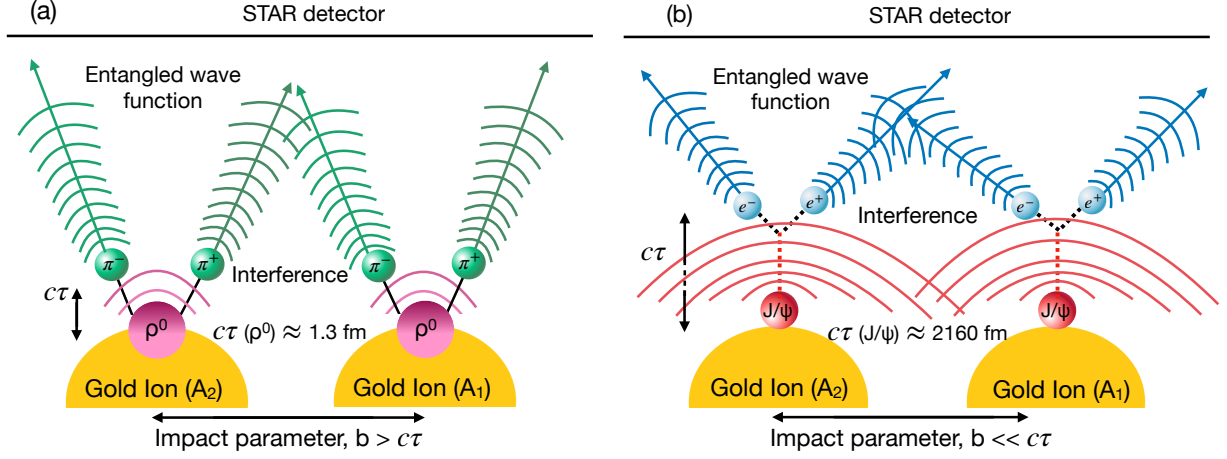


FIG. 1: Schematic comparison of quantum interference in coherent vector meson production in UPCs for a given impact parameter,  $b$ , at STAR. (a) For  $\rho^0 \rightarrow \pi^+\pi^-$ , the short lifetime ( $c\tau \approx 1.3$  fm [ $< b$ ]) leads to decay within the nuclear environment, limiting the spatial coherence. The spin-0 pions result in angular interference patterns that differ from those of leptonic decays. (b) In contrast, for  $J/\psi \rightarrow e^+e^-$ , the long lifetime ( $c\tau \approx 2160$  fm [ $\gg b$ ]) allows the meson to propagate far outside the nucleus before decaying. The final-state electrons are entangled, and interference arises between production amplitudes from the two nuclei.

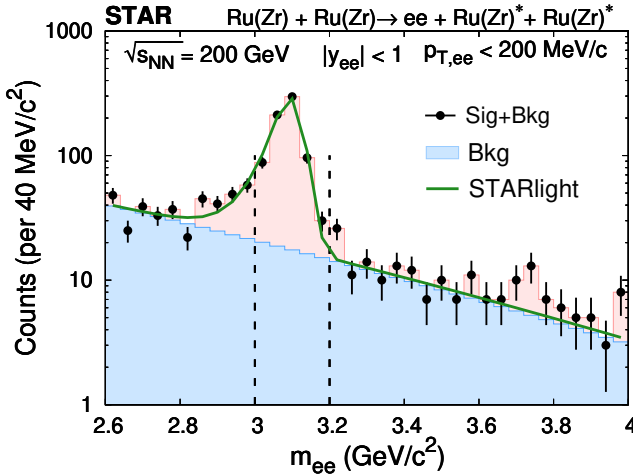


FIG. 2: Invariant mass  $m_{ee}$  distribution for  $e^+e^-$  pair candidates for pair transverse momentum  $p_{T,ee} < 200$  MeV/c and pair rapidity  $|y_{ee}| < 1$ , from Ru+Ru and Zr+Zr UPCs at  $\sqrt{s_{NN}} = 200$  GeV. The light red and blue regions are the distributions for unlike-sign ( $+-$ ) and like-sign ( $++$ ,  $--$ ) electron pairs, respectively. A template fit that includes STARlight coherent and incoherent  $J/\psi$  and QED processes is shown as the green curve. The two vertical black dashed curves represent the chosen  $J/\psi$  mass window,  $3 < m_{ee} < 3.2$  GeV/c<sup>2</sup>.

used to estimate the combinatorial background subsequently subtracted from the opposite-sign pairs to obtain the final signal distributions. The  $e^+e^-$  pair invariant mass ( $m_{ee}$ ) distributions for signal+background ( $+-$ ) and background ( $++$ ,  $--$ ) from Ru+Ru and Zr+Zr

UPCs at  $\sqrt{s_{NN}} = 200$  GeV are presented in Fig. 2. We also perform the same analysis for Au+Au UPCs at  $\sqrt{s_{NN}} = 200$  GeV.

For further analysis, we select the  $J/\psi$  decay candidate  $e^+e^-$  pairs in the range  $3 < m_{ee} < 3.2$  GeV/c<sup>2</sup>, and the pair  $p_T < 200$  MeV/c to measure the  $\phi$  observable using Eq. 2. The fits are made to the function  $1 + a_2 \cos(2\phi)$ , where  $a_2$  is the amplitude of the  $\cos(2\phi)$  modulation, the signal for spin interference. To correct the  $a_2$  signal for the combinatorial backgrounds as shown in Fig. 2, we decompose the measured  $a_2$  in a two component model:  $a_2^{\text{measured}} = f \times a_2^{\text{bkg}} + (1 - f) \times a_2^{\text{sig}}$ , with  $f = \frac{N_{\text{bkg}}}{N_{\text{sig}} + N_{\text{bkg}}}$  being the relative background yield ( $N_{\text{bkg}}$  is background counts,  $N_{\text{sig}} + N_{\text{bkg}}$  is total counts containing signal+background), obtained from the  $e^+e^-$  pair invariant mass distribution. The  $a_2^{\text{bkg}}$  is estimated from different mass bins on either side of the  $J/\psi$  signal region ( $3 < m_{ee} < 3.2$  GeV/c<sup>2</sup>). The corrections for detector effects and Bremsstrahlung processes are performed based on the STARlight [42] Monte Carlo events embedded into STAR zero-bias events. These combined events are then passed through a GEANT3-based [43] STAR detector simulation to model the detector response. In this simulation, STARlight includes coherent  $J/\psi$ , incoherent  $J/\psi$  (both with and without nucleon dissociation), as well as QED two-photon ( $\gamma\gamma$ ) processes. The Bremsstrahlung processes were included in the simulation, where the photons were generated with a bremsstrahlung energy spectrum [44]. To validate the simulation (the same as used in [11, 12]), templates of individual STARlight physics processes are used to fit  $m_{ee}$  and  $p_T$  distributions simultaneously with  $\chi^2$  minimization. Total template is shown

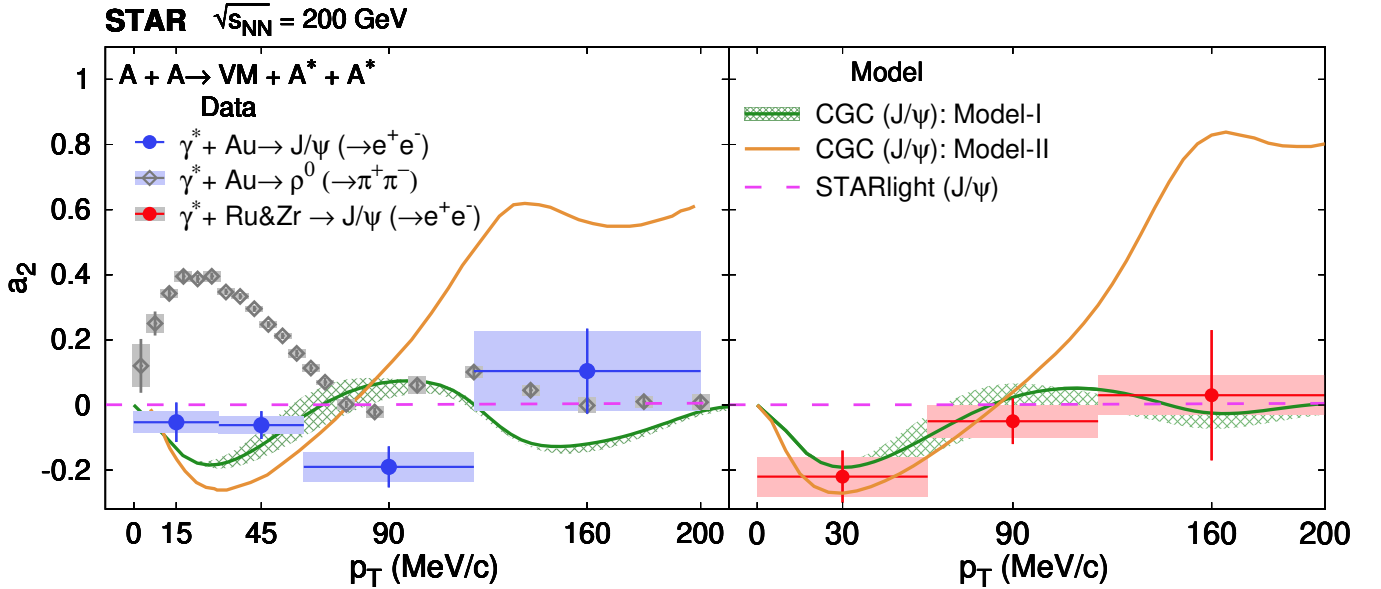


FIG. 3: The amplitude of the  $\cos(2\phi)$  modulation,  $a_2$ , as a function of  $J/\psi$   $p_T$  from Au+Au (left panel) and Ru+Ru & Zr+Zr (right panel) UPCs at  $\sqrt{s_{NN}} = 200$  GeV. The statistical uncertainty on each data point is shown as a vertical bar, while the systematic uncertainty is shown in the shaded band. The STARlight [42], CGC (Model-I) [7] and CGC (Model-II) [35] calculations are shown with magenta line, green band, and orange line, respectively. STARlight is used here as a spin-independent baseline and not as a full theoretical prediction of the modulation. Model-I incorporates CGC calculations with linear photon polarization and interference effects, while Model-II extends this framework by including soft-photon radiation in the final state.

in Fig. 2. The simulated events were selected using the same track and vertex criteria that were applied to the data. The measured  $a_2$  ( $a_2^M$ ) is the convolution of the true  $a_2$  signal ( $a_2^T$ ) and the effects of the detector. Assuming that the detector effects also produce a nonzero modulation amplitude  $a_2$  ( $a_2^D \neq 0$ ), the  $a_2^T$  can be obtained as [29]:  $a_2^T = \frac{a_2^M - a_2^D}{1 - 0.5a_2^M a_2^D}$ . The  $a_2^D$  is estimated from the aforementioned simulation productions. At low  $p_T$ , the back-to-back topology of  $J/\psi \rightarrow e^+e^-$  makes the reconstructed  $\phi$  distribution sensitive to azimuthal variations in acceptance and tracking efficiency, generating a nonzero detector modulation  $a_2^D$ . The magnitude and  $p_T$  dependence of  $a_2^D$  are determined from full embedding and applied bin-by-bin; following the standard STAR procedure established in azimuthal correlation analyses [45]. More details are provided in the Supplemental Material. The corrected  $a_2$  signal ( $a_2^T$ ) is presented in Fig. 3.

Systematic uncertainties are estimated by varying the event, track quality, and electron identification related selection criteria. Simulation parameters related to the  $p_T$  reweighting and smearing are also varied to investigate the systematic effects on  $a_2$ . Typical systematic uncertainties on the interference signal  $a_2$  due to the event, track, and topological selection criteria variations combined are below 6%, while that due to variations in sim-

ulation parameters is estimated to be under 12%. The data are corrected for TPC tracking efficiency and acceptance effects, with correction residuals included in the systematic uncertainty.

Figure 3 shows the measured interference signal  $a_2$  for  $J/\psi$  as a function of  $p_T$  from Au+Au and isobaric (Ru+Ru & Zr+Zr) UPCs at  $\sqrt{s_{NN}} = 200$  GeV. We compare the measured  $J/\psi$   $a_2$  with the published photoproduced  $\rho^0 \rightarrow \pi^+\pi^-$  results [29] in Au+Au UPCs at  $\sqrt{s_{NN}} = 200$  GeV. We observe a negative modulation for  $J/\psi$  both from Au+Au and isobaric UPCs, which is opposite in sign to the positive modulation reported for  $\rho^0$ . The interference effects damp out at large  $p_T$  where incoherent processes start to dominate. The measured values of  $J/\psi$   $a_2$  in  $p_T < 100$  MeV/c are  $-0.120 \pm 0.032$  (stat.)  $\pm 0.022$  (syst.) for Au+Au UPCs, and  $-0.123 \pm 0.061$  (stat.)  $\pm 0.045$  (syst.) for isobaric UPCs. The observed sign difference in the  $\cos(2\phi)$  modulation between  $J/\psi$  and  $\rho^0$  photoproduction provides direct evidence that the decay-channel spin structure controls the sign of the modulation within a common two-source interference mechanism:  $J/\psi \rightarrow e^+e^-$  (fermionic daughters) yields a negative modulation, whereas  $\rho^0 \rightarrow \pi^+\pi^-$  (bosonic daughters) exhibits a positive one [7, 35, 46]. Because both the  $\rho^0$  and its decay pions are bosons, the role of daughter spin is not apparent in the  $\rho^0$  channel alone; the  $J/\psi$  result makes this

dependence explicit even though the parent is a spin-1 boson.

The peak  $J/\psi$  modulation is smaller than that of the  $\rho^0$ , consistent with expectations [7] that its more compact dipole reduces the two-source overlap. At maximum, the modulation reaches  $-0.220 \pm 0.080$  (stat.)  $\pm 0.060$  (syst.) for the isobars and  $-0.190 \pm 0.063$  (stat.)  $\pm 0.044$  (syst.) for Au+Au, about half of the  $\rho^0$  peak.

The consistent negative modulation observed in both Au+Au and isobar systems highlights the robustness of spin-dependent interference in the fermionic  $J/\psi$  channel. Theoretical calculations indicate that the smaller radii of Ru and Zr are expected to strengthen the interference effect [7]. We observe that the signal strength for  $p_T < 60$  MeV/c is larger in the isobaric system, consistent with this geometric expectation (isobar  $|a_2| > \text{Au+Au } |a_2|$ ).

The data in Fig. 3 are compared to STARlight [42], which assumes no spin interference and therefore predicts  $a_2 = 0$ . In contrast, the CGC-based calculations (Model-I) [7], which include linear photon polarization, two-source interference, and finite photon transverse momentum, reproduce both the sign and approximate magnitude of the measured  $a_2$ . The agreement is noticeably better for isobars, while Au+Au data show a different  $p_T$  dependence, indicating further model refinement is needed for larger nuclei. The main Model-I uncertainty comes from the assumed impact-parameter range. The data are also compared to the CGC effective theory Model-II calculations [35], which extend the framework by incorporating final-state soft-photon radiation. This QED effect generates large positive  $a_2$  at higher  $p_T$ . Our data, which remain near zero in this region, do not support this large positive modulation, suggesting the soft-photon contribution is overestimated in the current calculation.

In summary, we observed spin interference in photo-produced  $J/\psi$  mesons in ultraperipheral collisions, exploiting their longer lifetime and delocalized wave function. Unlike  $\rho^0$ ,  $J/\psi$  exhibits a negative modulation for  $p_T < 100$  MeV/c, revealing an interference mechanism whose sign is governed by the two fermionic wave functions at a finite separation. As a heavier meson (3.1 GeV/c<sup>2</sup> vs. 0.77 GeV/c<sup>2</sup> for  $\rho^0$ ),  $J/\psi$  probes gluon distributions at finer spatial scales, making it stringent test of QCD effective theories like CGC. The smaller  $J/\psi$  peak amplitude relative to the  $\rho^0$  is consistent with theoretical expectations from its more compact dipole size. While current CGC calculations qualitatively capture the sign they do not fully reproduce the  $p_T$  dependence, highlighting the need for theoretical refinements.

These results also provide the first direct experimental evidence that polarization-driven angular interference in heavy vector mesons is measurable in photon-induced reactions. This finding directly supports recent proposals to exploit  $\cos(2\phi)$  modulations in  $J/\psi$  decays as a

powerful imaging tool in diffractive  $e+A$  scattering at the Electron-Ion-Collider [47]. Together, these developments highlight angular spin interference as a new degree of freedom for resolving gluon spatial structure, beyond what is accessible through  $t$ -dependent cross sections alone.

### Acknowledgment

We thank the RHIC Operations Group and SDCC at BNL, the NERSC Center at LBNL, and the Open Science Grid consortium for providing resources and support. This work was supported in part by the Office of Nuclear Physics within the U.S. DOE Office of Science, the U.S. National Science Foundation, National Natural Science Foundation of China, Chinese Academy of Science, the Ministry of Science and Technology of China and the Chinese Ministry of Education, NSTC Taipei, the National Research Foundation of Korea, Czech Science Foundation and Ministry of Education, Youth and Sports of the Czech Republic, Hungarian National Research, Development and Innovation Office, New National Excellency Programme of the Hungarian Ministry of Human Capacities, Department of Atomic Energy and Department of Science and Technology of the Government of India, the National Science Centre and WUT ID-UB of Poland, the Ministry of Science, Education and Sports of the Republic of Croatia, German Bundesministerium für Bildung, Wissenschaft, Forschung und Technologie (BMBF), Helmholtz Association, Ministry of Education, Culture, Sports, Science, and Technology (MEXT), Japan Society for the Promotion of Science (JSPS) and Agencia Nacional de Investigación y Desarrollo (ANID) of Chile.

### SUPPLEMENTAL MATERIAL: CORRECTIONS DUE TO DETECTOR EFFECT

To quantify detector-induced modulations in the  $\phi$  distribution, we use STARlight  $J/\psi \rightarrow e^+e^-$  UPC events with no physical  $\cos(2\phi)$  input ( $a_2^T = 0$ ). The events are embedded into zero-bias data and processed through the full GEANT3 simulation and STAR reconstruction chain, with identical selections to those used for data. This procedure, widely employed in recent STAR analyses [45], provides a realistic estimate of the detector response.

The reconstructed  $\phi$  spectra in each  $p_T$  bin are fitted using

$$N(\phi) = A[1 + a_2^D \cos(2\phi)],$$

yielding a bin-by-bin determination of  $a_2^D$ . For illustration, Fig. 4 shows the reconstructed distributions for two low- $p_T$  bins.

From these fits we extract  $a_2^D = -0.0781 \pm 0.0091$  for  $p_T < 30$  MeV/ $c$  and  $a_2^D = 0.0275 \pm 0.0068$  for  $30 < p_T < 60$  MeV/ $c$ . These values quantify the detector response that is removed via the correction formula described in the main text. No physical conclusions are drawn from the magnitude of  $a_2^D$  itself; only the corrected observable  $a_2^T$  is used in the physics interpretation.

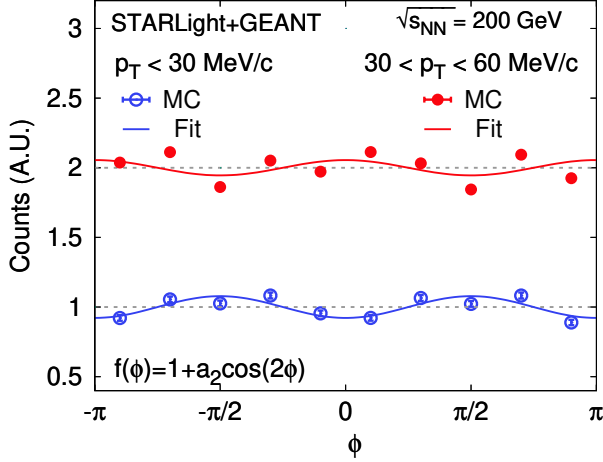


FIG. 4: Detector-only  $\phi$  modulation from STARlight+GEANT with STARlight input  $a_2^{\text{true}} = 0$ . STARlight points are first embedded into zero-bias data, then a full GEANT3-based reconstruction is performed. We refer to this as “MC”. The curves are fit to the MC points with  $1 + a_2^D \cos(2\phi)$ .

[1] R. Abdul Khalek et al., Nucl. Phys. A **1026**, 122447 (2022).  
[2] C. A. Bertulani, S. R. Klein, and J. Nystrand, Ann. Rev. Nucl. Part. Sci. **55**, 271 (2005).  
[3] S. R. Klein and H. Mäntysaari, Nature Rev. Phys. **1**, 662 (2019).  
[4] H. Mäntysaari and B. Schenke, Phys. Rev. Lett. **117**, 052301 (2016).  
[5] H. Mäntysaari and B. Schenke, Phys. Rev. D **94**, 034042 (2016).  
[6] H. Mäntysaari, F. Salazar, and B. Schenke, Phys. Rev. D **106**, 074019 (2022).  
[7] H. Mäntysaari, F. Salazar, B. Schenke, C. Shen, and W. Zhao, Phys. Rev. C **109**, 024908 (2024).  
[8] H. Mäntysaari, B. Schenke, C. Shen, and W. Zhao, Phys. Lett. B **833**, 137348 (2022).  
[9] S. Afanasiev et al. (PHENIX), Phys. Lett. B **679**, 321 (2009).  
[10] L. Adamczyk et al. (STAR), Phys. Rev. C **96**, 054904 (2017).  
[11] M. I. Abdulhamid et al. (STAR), Phys. Rev. Lett. **133**, 052301 (2024).  
[12] M. I. Abdulhamid et al. (STAR), Phys. Rev. C **110**, 014911 (2024).

[13] V. Khachatryan et al. (CMS), Phys. Lett. B **772**, 489 (2017).  
[14] B. Abelev et al. (ALICE), Phys. Lett. B **718**, 1273 (2013).  
[15] S. Acharya et al. (ALICE), JHEP **06**, 035 (2020).  
[16] S. Acharya et al. (ALICE), Phys. Lett. B **820**, 136481 (2021).  
[17] S. Acharya et al. (ALICE), Phys. Lett. B **817**, 136280 (2021).  
[18] S. Acharya et al. (ALICE), Eur. Phys. J. C **81**, 712 (2021).  
[19] R. Aaij et al. (LHCb), Phys. Rev. C **105**, L032201 (2022).  
[20] A. Tumasyan et al. (CMS), Phys. Rev. Lett. **131**, 262301 (2023).  
[21] S. Acharya et al. (ALICE), JHEP **10**, 119 (2023).  
[22] M. G. Ryskin, Z. Phys. C **57**, 89 (1993).  
[23] S. Klein and J. Nystrand, Phys. Rev. C **60**, 014903 (1999).  
[24] S. Munier, A. M. Stasto, and A. H. Mueller, Nucl. Phys. B **603**, 427 (2001).  
[25] V. Guzey, E. Kryshen, and M. Zhalov, Phys. Rev. C **93**, 055206 (2016).  
[26] J. Adam et al. (STAR), Phys. Rev. Lett. **127**, 052302 (2021).  
[27] W. Zha, J. D. Brandenburg, L. Ruan, Z. Tang, and Z. Xu, Phys. Rev. D **103**, 033007 (2021).  
[28] W. Zha, L. Ruan, Z. Tang, Z. Xu, and S. Yang, Phys. Rev. C **99**, 061901 (2019).  
[29] M. Abdallah et al. (STAR), Sci. Adv. **9**, eabq3903 (2023).  
[30] S. R. Klein and J. Nystrand, Phys. Rev. Lett. **84**, 2330 (2000).  
[31] H. Xing, C. Zhang, J. Zhou, and Y.-J. Zhou, JHEP **10**, 064 (2020).  
[32] S. Acharya et al. (ALICE), Phys. Lett. B **858**, 139017 (2024).  
[33] S. R. Klein and J. Nystrand, Phys. Lett. A **308**, 323 (2003).  
[34] J. D. Brandenburg, H. Duan, Z. Tu, R. Venugopalan, and Z. Xu, Phys. Rev. Res. **7**, 013131 (2025).  
[35] J. D. Brandenburg, Z. Xu, W. Zha, C. Zhang, J. Zhou, and Y. Zhou, Phys. Rev. D **106**, 074008 (2022).  
[36] K. H. Ackermann et al. (STAR), Nucl. Instrum. Meth. A **499**, 624 (2003).  
[37] M. Anderson et al., Nucl. Instrum. Meth. A **499**, 659 (2003).  
[38] M. Beddo et al. (STAR), Nucl. Instrum. Meth. A **499**, 725 (2003).  
[39] J. Chen et al., Nucl. Sci. Tech. **35**, 214 (2024), 2407.02935.  
[40] C. A. Whitten (STAR), AIP Conf. Proc. **980**, 390 (2008).  
[41] Y.-F. Xu, J.-H. Chen, Y.-G. Ma, A.-H. Tang, Z.-B. Xu, and Y.-H. Zhu, Nucl. Sci. Tech. **27**, 126 (2016).  
[42] S. R. Klein, J. Nystrand, J. Seger, Y. Gorbunov, and J. Butterworth, Comput. Phys. Commun. **212**, 258 (2017).  
[43] R. Brun, F. Bruyant, M. Maire, A. C. McPherson, and P. Zanzarini (CERN-DD-EE-84-1 (1987)).  
[44] K. A. Olive et al. (Particle Data Group), Chin. Phys. C **38**, 090001 (2014).  
[45] M. I. Abdulhamid et al. (STAR), Phys. Rev. C **111**, 014906 (2025), 2406.18213.  
[46] Y. Hagiwara, C. Zhang, J. Zhou, and Y.-J. Zhou, Phys. Rev. D **103**, 074013 (2021).  
[47] M. Kesler, A. I. Sheikh, R. Ma, Z. Tu, T. Ullrich, and

Z. Xu (2025), 2502.15596.